Application of Aeroservoelastic Modeling Using Minimum-State Unsteady Aerodynamic Approximations

Sherwood T. Hoadley*
NASA Langley Research Center, Hampton, Virginia 23665
and
Mordechay Karpel†
Technion—Israel Institute of Technology, Haifa, 32000 Israel

Various control analysis, design, and simulation techniques for aeroservoelastic applications require the equations of motion to be cast in a linear time-invariant state-space form. Unsteady aerodynamic forces have to be approximated as transfer functions of the Laplace variable in order to put them in this framework. For the minimum-state method, the number of augmenting states representing the unsteady aerodynamics is a function only of the number of denominator roots in the approximation. Results are shown of applying various approximation enhancements (including optimization, mode, and frequency-dependent weighting of the tabular data, and constraint selection) of a minimum-state formulation of the equations of motion of an active flexible wing wind-tunnel model. The results demonstrate that good mathematical models can be developed which have a factor of 10 fewer augmenting aerodynamic equations than more traditional approaches. This reduction facilitates the design of lower-order control systems, analysis of control system performance, and near real-time simulation of aeroservoelastic phenomena.

Nomenclature

$[A_m]$ = numerator coefficient matrix for rational function approximations defined by Eq. (1)
c = reference chord, typically mean aerodynamic chord
$[D]$, $[E]$ = coupled numerator coefficient matrices in minimum-state approximation
$[G]$ = damping matrix in equations of motion
$[K]$ = stiffness matrix in equations of motion
k = reduced frequency, $(c/2u)\omega$
k_n = a tabulated reduced frequency
k' = modal reduced frequencies when system goes unstable
$[M]$ = mass matrix in equations of motion
n_ξ = number of structural modes
p = nondimensionalized Laplace variable, $(c/2n)s$
Q_{ij} = generalized unsteady aerodynamic force coefficient
$\hat{Q}_{ij}(ik)$ = approximate value of $Q_{ij}(ik)$
$Q_{ij}(ik_n)$ = tabular value of Q_{ij} at a specified value of reduced frequency, k_n
q = dynamic pressure
$[R]$ = diagonal matrix of aerodynamic roots
s = Laplace variable
u = freestream velocity
w_{cut} = minimum of the maximum weighted amplitude of the tabular values of an aerodynamic coefficient
w_{ijn} = weights assigned to approximation error of $Q_{ij}(ik_n)$
$\bar{w}_{ijn}$ = "measure-of-importance" of $Q_{ij}(ik_n)$ based on open-loop sensitivity
w_{ij}^* = normalizing weight defined by Eq. (10)
X_a = vector of augmenting aerodynamic states
α_g = nondimensional gust velocity
δ = control mode
$\epsilon_{ij}(ik_n)$ = approximation error between two corresponding points
ϵ_t = total weighted error, defined by Eq. (6)
ϵ_{t_N} = total normalized error, defined by Eqs. (6) and (10)
ϵ_{t_0} = total physically weighted error, defined by Eqs. (6) and (15) with $w_{cut} = 0$
ω = frequency
ω' = modal frequencies when system goes unstable
ξ = structural mode

Subscripts
g = gust mode
δ = control mode
ξ = structural mode

Symbols
$|\cdot|$ = magnitude of $\cdot$
$\|\cdot\|$ = determinant of $\cdot$

Introduction

EQUATIONS of motion of a flexible aircraft include unsteady generalized aerodynamic force terms that contain transcendental functions. Approximating the unsteady aerodynamic forces as rational functions of the Laplace variable, i.e., ratios of polynomials that may be referred to as aerodynamic transfer functions, allows efficient linear systems algorithms to be used in aeroservoelastic analysis and design of active control systems for flutter suppression, gust load alleviation, and maneuver load alleviation of flexible air-

Presented as Paper 89-1188 at the AIAA Structures, Structural Dynamics, and Materials Conference, Mobile, AL, April 3–5, 1989; received Sept. 6, 1989; revision received July 16, 1990; accepted for publication Oct. 2, 1990.

*Senior Aerospace Engineer, Aeroservoelasticity Branch, Structural Dynamics Division, Mail Stop 243. Associate Fellow AIAA.
†Senior Research Fellow, Department of Aerospace Engineering. Member AIAA.

craft.[1-5] The rational function approximations (RFAs) are used to define the aeroservoelastic equations of motion in a linear time invariant (LTI) state-space form, albeit with increased size of the state vector due to the RFAs. This increase in the number of states due to the RFAs is referred to herein as the aerodynamic dimension. There is always a tradeoff between how well the RFAs approximate the aerodynamic forces and the desire to keep the aerodynamic dimension small. The RFA formulations in Refs. 1-14 have varying capabilities to perform such a tradeoff.

Currently there are three basic formulations used in these references to approximate unsteady generalized aerodynamic forces for arbitrary motion using rational functions: 1) least-squares (LS)[1,5,9-12]; 2) modified matrix-Padé (MMP)[2,3,6,7]; and 3) minimum-state (MS).[8,11-14] Extensions to these approaches were developed[9-14] which included the capability to enforce selected equality constraints on the RFAs and of optimizing the denominator coefficients in the rational functions using nonlinear programming techniques. For the minimum-state method, the number of augmenting states required to represent the unsteady aerodynamics is a function only of the number of denominator roots in the rational approximation; there are no repeated aerodynamic roots as there are for the LS formulation. Methods to determine critical frequency ranges based on physical properties and to determine weightings of the individual tabular errors to improve approximations in those critical regions have been explored in Refs. 13 and 14.

The evolution of advanced fighters has required that the aerodynamics, control systems, and structures disciplines be integrated into a unified aeroservoelastic technology, evaluated by sophisticated analytical methods, and validated through the testing of wind-tunnel models. The active flexible wing (AFW) wind-tunnel model is a scaled aeroservoelastic model designed and built specifically as a research vehicle for testing multi-input/multi-output digital control laws for flutter suppression and rolling maneuver load alleviation.[15,16] The purpose of this paper is to demonstrate the various MS aerodynamic modeling techniques by applying them to a current mathematical model in order to develop valid low-order state-space equations for the control system design, evaluation, and near real-time simulation.

The following presents a brief description of the techniques involved. Results are also shown which demonstrate that models can be developed which have one tenth the number of aerodynamic state equations than more traditional approaches without sacrificing the flutter and frequency response characteristics of the higher-order systems.

Unsteady Aerodynamic Approximations

Aeroservoelastic modeling starts with a definition of structural, control, and gust modes that are used as generalized coordinates. In this work, the structural modes are a set of low-frequency vibration modes, the control modes are defined by unit rotations of each control surface, and the gust modes by complex displacement vectors that simulate the encounter of sinusoidal gusts. The modes are then used to calculate generalized unsteady force coefficient matrices that reflect the aerodynamic coupling between the oscillating modes.

To express the equations of motion in first-order form, the unsteady generalized aerodynamic force (GAF) coefficients Q_{ij} must be defined in the complex Laplace s domain, or nondimensionalized Laplace p domain. Since the GAF coefficients are computed at specified values of reduced frequencies k_n, it is necessary to generate complex p-domain functions by approximating the tabular values, $Q_{ij}(ik_n)$, of the GAFs as closely as possible, and then employ the concept of analytic continuation in a region near the imaginary axis. Figure 1 depicts the approximating process for a single element Q_{ij} of Q, where the tabulated data, $Q_{ij}(ik_n)$, are denoted by the open circles, the corresponding approximated values, $\hat{Q}_{ij}(ik_n)$, are denoted by solid dots, and the approximating

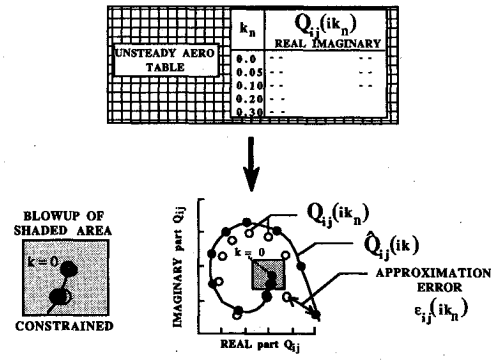

Fig. 1 Approximating aerodynamic tabular data for a single element of Q, employing constraints.

frequency-domain curve by the solid line. The approximation error, $\epsilon_{ij}(ik_n)$, between two corresponding points is denoted by an arrow between the points.

The approximating function, $\hat{Q}_{ij}(p)$, is determined in such a way as to minimize some least-squares combination of the errors, $\epsilon_{ij}(ik_n) = |\hat{Q}_{ij}(ik_n) - Q_{ij}(ik_n)|$, between the approximating function at $p = ik_n$ and the tabular value $Q_{ij}(ik_n)$. It is possible that certain equality constraints or weighted constraints might be desirable to impose on some of the tabular values [such as the steady-state ($k = 0$) point, shown in the shaded box].

Review of Rational Function Approximations to Generalized Aerodynamic Forces

The most common form of the approximating functions used currently for each generalized force coefficient, Q_{ij}, is a rational function of the nondimensional Laplace variable p. A common form chosen is one in which the numerator polynomial is order two more than the denominator. This gives rise to the following partial-fraction form for each element Q_{ij}:

$$\hat{Q}_{ij}(p) = (A_0)_{ij} + (A_1)_{ij}\, p + (A_2)_{ij}\, p^2 + \hat{Q}_{L_{ij}}(p) \qquad (1)$$

where $\hat{Q}_{L_{ij}}$ is a finite sum of ratios of first-order polynomials of the variable p. The fundamental difference between the aerodynamic approximation methods are in the formulation of this term. Expressions for this term in the LS, MMP, and MS methods, and associated aerodynamic dimensions are given in Table 1 and discussed below. Equation (1) can be rewritten in the Laplace domain by replacing p with $(c/2u)s$.

Because tabular data are determined for specified values of reduced frequency k_n, the Q_{ij} are actually defined only for

Table 1 RFA matrix formulations

Aerodynamic method	Character of $\hat{Q}_L$	Aerodynamic dimension
Least-squares	Common denominator coefficients in each $\hat{Q}_{ij}$ $\hat{Q}_{L_{ij}} = \sum_{n=1}^{n_L} [A_{(n+2)}]_{ij} \frac{p}{p + b_n}$	$n_\xi \cdot n_L$
Modified matrix-Padé	Different number of and values for denominator coefficients for each column, Q_j $\hat{Q}_{L_{ij}} = \sum_{n=1}^{n_{Lj}} [A_{(n+2)}]_{ij} \frac{p}{p + b_{n_j}}$	$\sum_{j=1}^{n_\xi + n_g} n_{L_j}$
Minimum-state	Common denominator coefficients in each $\hat{Q}_{ij}$ $\hat{Q}_{L_{ij}} = \sum_{n=1}^{N} \frac{D_{in} E_{nj} p}{p + b_n}$	N

these values of the nondimensionalized Laplace variable $p = ik_n$. The coefficients of the approximating functions are found by least-squares procedures that vary according to the character of $\hat{Q}_L$. The coefficients are then used to construct the linear, time-invariant, state-space aeroservoelastic equations of motion. The fact that the common numerator of Eq. (1) is only of order two more than the common denominator implies the number of resulting equations associated with the aerodynamics is a function of the order of the common denominator polynomial. The A_0, A_1, and A_2 terms can be included with the stiffness, damping, and mass terms, without any additional equations. The terms of $\hat{Q}_{L_{ij}}$ are commonly called lag terms because they represent a transfer function in which the output lags the input and permits an approximation of the time delays inherent in unsteady aerodynamics.

The matrix form of the LS approximation (the first in Table 1) is

$$[\hat{Q}(p)] = [A_0] + [A_1]\,p + [A_2]\,p^2 + [\hat{Q}_L] \tag{2}$$

where

$$[\hat{Q}_L] = \sum_{n=1}^{n_L} \{[A_{(n+2)}]\}\,\frac{p}{p + b_n}$$

The number and values of denominator coefficients, b_n, are fixed for all $\hat{Q}_{ij}$. For a given set of values, the A_m coefficients of Eq. (2) are calculated by simple term-by-term least-squares solutions. The number of aerodynamic augmenting states in the resulting state-space model is n_L times n_ξ (see Ref. 10).

The column vector form of the MPP approximation (the second in Table 1) is:

$$\hat{Q}_j(p) = \{A_0\}_j + \{A_1\}_j\,p + \{A_2\}_j\,p^2 + \hat{Q}_{Lj} \tag{3}$$

where

$$\hat{Q}_{Lj} = \sum_{n=1}^{n_{Lj}} \{A_{n+2}\}\,\frac{p}{p + b_{n_j}}$$

which allows the number of denominator coefficients and their values to vary between columns. They are only fixed per column. For a given set of b_{n_j} values, the associated A_m coefficients are also calculated by simple least-squares solutions. The number of resulting augmenting aerodynamic states is equal to the sum of the number of b_{n_j} values associated with each structural, control, and gust mode.[10-12]

The matrix form of the MS approximation (the last in Table 1) is

$$[\hat{Q}(p)] = [A_0] + [A_1]\,p + [A_2]\,p^2 + [\hat{Q}_L] \tag{4}$$

where

$$[\hat{Q}_L] = [D](p[I] - [R])^{-1}[E]p$$

which fixes the denominator coefficients as in the least-squares to be the same for all $\hat{Q}_{ij}$, but additionally, the partial-fraction numerator coefficients are determined as a coupled product of a premultiplying matrix $[D]$ and a postmultiplying matrix $[E]$. The diagonal matrix of aerodynamic roots, chosen a priori, is denoted by $[R]$; i.e.,

$$[R] = \begin{bmatrix} \ddots & & \\ & -b_n & \\ & & \ddots \end{bmatrix}, \quad n = 1, \ldots, N \tag{5}$$

Detailed development of the MS formulation and subsequent construction of the aeroservoelastic model are given in Refs. 8 and 13. As shown in the next section, the resulting number of aerodynamic states introduced into the first-order equations as a result of the MS formulation is N [the order of R in Eq. (5)]. This is the main advantage of the MS formulation. Even though N is usually a little larger than n_L [the number of partial fractions in the LS and MMP expressions of Eqs. (2) and (3)] it is generally much smaller than the aerodynamic dimension resulting from the LS and MMP formulations per given level of model accuracy, where model accuracy is based on various criteria described later in this paper.

For a given set of b_n values, the MS numerator coefficient matrices $[A_0]$, $[A_1]$, $[A_2]$, $[D]$, and $[E]$ are determined using iterative, nonlinear least-squares methods that minimize an overall error function,

$$\epsilon_t = \sqrt{\sum_{i,\,j,\,n} \epsilon_{ij}^2\,(ik_n) w_{ijn}^2} \tag{6}$$

where w_{ijn} are the weights assigned to the tabulated data terms. The iterative technique assumes an initial $[D]$, determines $[A_0]$, $[A_1]$, $[A_2]$, and $[E]$ using least-squares methods, then uses the current $[A_0]$, $[A_1]$, $[A_2]$, and $[E]$ to determine a new $[D]$ using least-squares methods. This process is continued until coefficient matrices are found which give a converged minimum error. Various implementations of this process are detailed in Refs. 8–14.

Constraints and Lag Coefficient Optimization

It is often desirable to impose constraints on the approximating functions or to determine an optimal set of denominator coefficients (aerodynamic roots) for the approximating functions. Various enhancements of the LS, MMP, and MS methods include capabilities to select equality constraints and to perform a nonlinear optimization of the denominator coefficients.[9-14] The equality constraints allow for more realistic modeling of the aerodynamics and for improved fits at critical points (such as flutter). Equality constraints can be used to reduce the number of unknowns in the iterative least-squares process; i.e., they can be used to explicitly solve for $[A_0]$, $[A_1]$, and $[A_2]$, thus reducing the size of each least-squares solution. For the MS method the solution process in Refs. 8, 13, and 14 requires the imposition of three equality constraints on each element Q_{ij} to reduce the size of each least-squares solution to that of the rank of R.[8] One constraint is data match at $k = 0$ and the others are real-part data match at a nonzero tabulated k_n [which can be replaced by enforcing $A_2 = 0$ in Eq. (4)] and an imaginary data match (which can be replaced by enforcing $A_1 = 0$). The solution of Refs. 9–12 allows flexibility in the number as well as the type of contraints selected, but the tradeoff in computational time for the MS solution is severe because the explicit solution for $[A_0]$, $[A_1]$, and $[A_2]$ is not performed for all types of constraints.

As shown in Refs. 9–12, nonlinear optimization of the denominator roots (b_n values) allows improvement in the approximations without increasing their number by determining a better set of coefficients than might be chosen a priori, even using some reasonable engineering strategy. Although application of root optimization to the MS solution process therein is severe for the reasons described in the preceding paragraph, when used in conjunction with the solution process of Refs. 8, 13, and 14, the increase in computational costs is not severe since the size of each least-squares solution is rank $[R]$. However, the aerodynamic dimension for the MS formulation tends to be much smaller than for either the LS or MMP formulations; therefore a larger number of b_n values can be used without much increase in the size and cost of state-space analyses. This reduces the advantages of root optimization which were shown for the LS and MMP formulations in Refs. 9–12. In the AFW application herein, it is shown that two optimized b_n values give almost identical results as four unoptimized b_n values, but for the MS state-space formulation, this only reduces the number of equations to be solved by two. For the LS and MMP formulations of the same model, this would result in 22 fewer equations.

The capability to include weights, w_{ijn}, on each $\epsilon_{ij}(ik_n)$, to either weight the importance of the fits for each tabular point, $Q_{ij}(ik_n)$, or to normalize the fits, can be considered a weight-

ing constraint. The determination of these weights based upon physical properties of the system is referred to as physical weighting, and is described later in this paper.

Minimum-State Equations of Motion

The approximated aerodynamic matrix of Eq. (4) has, in the application of this work, the dimensions of $n_\xi \times (n_\xi + n_\delta + n_g)$, and the matrix can be partitioned into structural, control, and gust related columns:

$$[\hat{Q}(p)] = [\hat{Q}_\xi \vdots \hat{Q}_\delta \vdots \hat{Q}_g] \tag{7}$$

which yields similar partitions of the $[A_0]$, $[A_1]$, $[A_2]$, and $[E]$ matrices. The generalized stiffness, damping, and mass matrices $[K]$, $[G]$, and $[M]$ can be partitioned similarly, where $[K_\xi]$, $[G_\xi]$, and $[M_\xi]$ are associated with structural modes only; $[K_\delta]$, $[G_\delta]$, and $[M_\delta]$ reflect the coupling between structures and control modes, and $K_g = G_g = M_g = 0$.

A vector of augmenting aerodynamic states defined by its Laplace transform as

$$\{X_a(s)\} = \big(s[I] - (2u/c)[R]\big)^{-1} s\big([E_\xi]\{\xi(s)\} + [E_\delta]\{\delta(s)\} + [E_g]\{\alpha_g(s)\}\big) \tag{8}$$

where $[\xi]$, $[\delta]$, and $[\alpha_g]$ represent the structural, control, and induced gust angle-of-attack modes. Equations (4), (7), (8), and Newton's equation of motion then yield the following open-loop time-domain state-space equations of motion:

$$\begin{Bmatrix} \dot{\xi} \\ \ddot{\xi} \\ \dot{X}_a \end{Bmatrix} = \begin{bmatrix} 0 & I & 0 \\ -\bar{M}_\xi^{-1}\bar{K}_\xi & -\bar{M}_\xi^{-1}G_\xi & q\bar{M}_\xi^{-1}D_\xi \\ 0 & E_\xi & (2u/c)R \end{bmatrix} \begin{Bmatrix} \xi \\ \dot{\xi} \\ X_a \end{Bmatrix} + \begin{bmatrix} 0 & 0 & 0 \\ -\bar{M}_\xi^{-1}\bar{K}_\delta & -\bar{M}_\xi^{-1}\bar{G}_\delta & -\bar{M}_\xi^{-1}\bar{M}_\delta \\ 0 & E_\delta & 0 \end{bmatrix} \begin{Bmatrix} \delta \\ \dot{\delta} \\ \ddot{\delta} \end{Bmatrix} + \begin{bmatrix} 0 & 0 \\ -\bar{M}_\xi^{-1}\bar{K}_g & -\bar{M}_\xi^{-1}\bar{G}_g \\ 0 & E_g \end{bmatrix} \begin{Bmatrix} \alpha_g \\ \dot{\alpha}_g \end{Bmatrix} \tag{9}$$

where

$$[\bar{M}] = [M] - q\left(\frac{c}{2u}\right)^2[A_2]$$

$$[\bar{K}] = [K] - q[A_0]$$

$$[\bar{G}] = [G] - q\frac{c}{2u}[A_1]$$

The full development of Eq. (9) is given in Ref. 8. This equation is the basis for stability, response, performance, and control analyses.

Physical Weighting

In most existing aerodynamic RFA methods, such as those reviewed in Refs. 11 and 12, all of the tabulated aerodynamic terms are treated equally importantly except for those chosen to be matched by the approximation at selected reduced frequencies. In addition to forcing the actual approximation to meet equality constraints, it is possible to weight some of the individual errors, $\epsilon_{ij}(ik_n)$, by w_{ijn} to be more important than others in the LS solution; thus, the fits can be improved in some frequency regions (at the possible expense of others) without enforcing additional equality constraints. The question of how to determine these weights must then be addressed. In Refs. 9–12, the weights provide a form of data normalization; i.e., each weight $w_{ijn} = w_{ij}^*$ where

$$w_{ij}^* = \frac{1}{\max\{\max_n |Q_{ij}(ik_n)|, 1\}} \tag{10}$$

A true test for a good approximation would be in the accuracy of the aeroservoelastic model in subsequent analyses. Hence, it is desirable to weight the aerodynamic data terms according to their influence on fundamental aeroservoelastic characteristics; i.e., the higher the sensitivity of critical aeroservoelastic characteristics is to errors in the approximation of a particular aerodynamic data term, the higher its weight. In Refs. 13 and 14, a systematic physical weighting procedure is developed in which each tabulated data term is assigned a "measure-of-importance," $\bar{w}_{ijn}$, based upon the sensitivity of open-loop characteristics at a specified design point to errors in the fit of each tabular point. The following is a brief development of the weighting equations.

For the structural modes, the weight of the fit for a particular aerodynamic data term, $Q_{\xi_{ij}}(ik_n)$, is based upon the derivative of the frequency-domain system matrix determinant with respect to this term:

$$\frac{\partial \|C_\xi(ik_n)\|}{\partial Q_{\xi_{ij}}(ik_n)} = -\bar{q} \times \text{cofactor } [C_{\xi_{ij}}(ik_n)] \tag{11}$$

where

$$[C_\xi(ik_n)] = -[M_\xi]\left(\frac{2u}{c}k\right)^2 + i[G_\xi]\frac{2u}{c}k + [K_\xi] - \bar{q}[Q_\xi(ik_n)]$$

and $\bar{q}$ is a nominal dynamic pressure chosen for the weighting. It is demonstrated in Ref. 13 that the accuracy of the resulting model is not very sensitive to the choice of $\bar{q}$, providing $[C_\xi(ik_n)]$ is not too close to a singularity. The division of Eq. (11) by $\|C_\xi(ik_n)\|$ yields a measure-of-importance matrix

$$[\bar{w}_\xi]_n = \bar{q}\,|[C_\xi(ik_n)]^{-1}|^T \tag{12}$$

For control modes, the weight of the fit for $Q_{\delta_{ij}}(ik_n)$ is based on the effect of a small error in this term upon the open-loop output response of the jth actuator to sinusoidal excitation by the jth control surface. This leads to the measure-of-importance matrix

$$[\bar{w}_\delta]_n = \bar{q}\,|[T(ik_n)][\Psi_m][C_\xi(ik_n)]^{-1}| \tag{13}$$

where $[T(ik_n)]$ is the matrix of transfer functions from sensor inputs to actuator outputs and $[\Psi_m]$ is a matrix of modal deflections or rotations at the sensor locations.

The weight of the fit for a term $Q_{g_{ij}}(ik_n)$ in a gust column is based on the error effects on the acceleration response of a chosen structural point to sinusoidal excitation. The resulting measure-of-importance vector is

$$\{\bar{w}_g\}_n = \frac{4\bar{q}uk_n^2}{c^2}\left|\{\Psi_m\}[C_\xi(ik_n)]^{-1}\right|^T\sqrt{\Phi_g(k_n)} \tag{14}$$

where $\{\Psi_m\}$ is a vector of modal displacements at the chosen point and Φ_g is the power spectral density of the gust velocity.

The measure-of-importance matrices are used to calculate the weights assigned in the least-squares solutions to a tabulated $Q_{ij}(ik_n)$ term of a certain partition by

$$w_{ijn} = \bar{w}_{ijn}\left(\max\left\{\frac{1}{\max_{ij}\{\tilde{w}_{ij}\}}, \frac{w_{cut}}{\tilde{w}_{ij}}\right\}\right) \tag{15}$$

where $\tilde{w}_{ij} = \max_n\{|Q_{ij}(ik_n)|\bar{w}_{ijn}\}$, w_{cut} is a user selected value, $0 \le w_{cut} \le 1$, and the $\bar{w}_{ijn}$ are defined by either Eqs. (12), (13), or (14), depending on whether j represents a structural mode, a control mode, or a gust mode.

Numerical difficulties may arise when all of the $\bar{w}_{ijn}$ weights assigned to a single Q_{ij} term are small. The w_{cut} in Eq. (15) provides a means to upscale these weights since the maximum

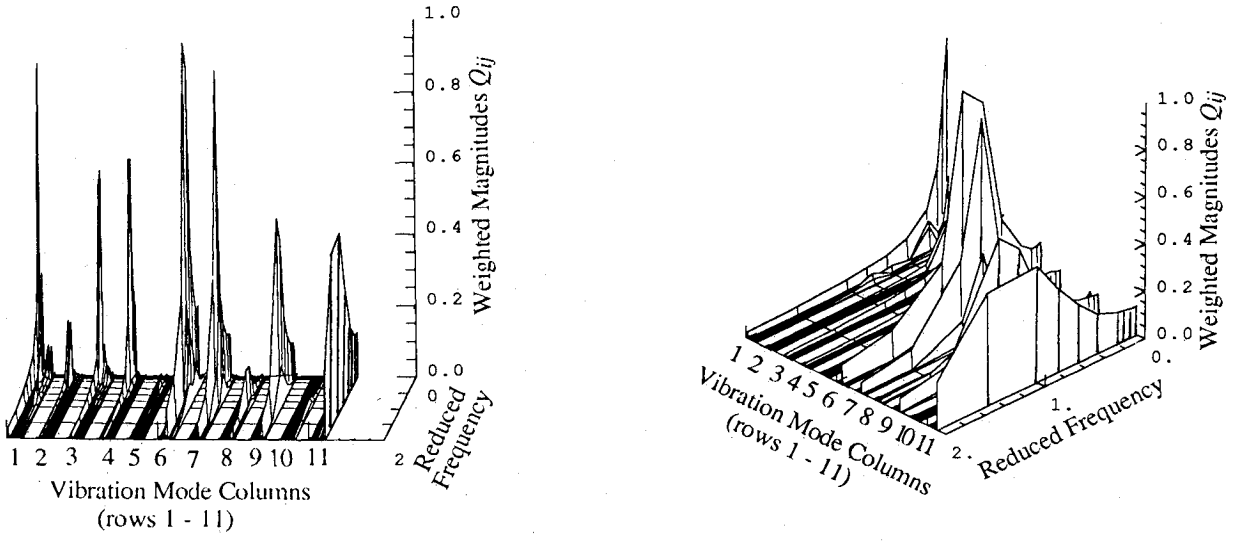

a) Vibration modes and rigid body roll

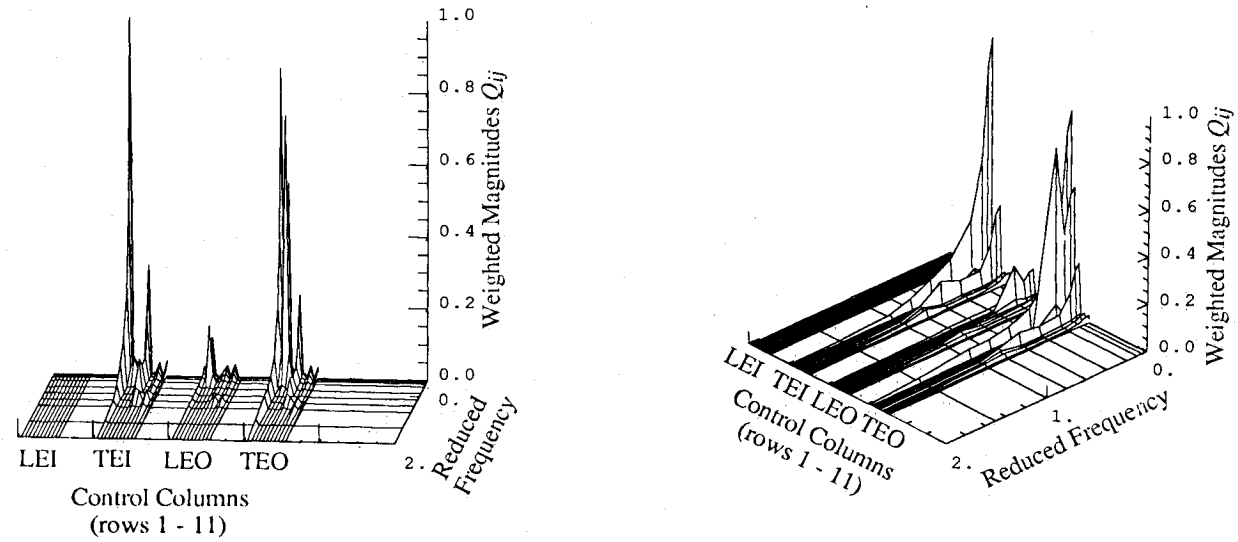

b) Control modes

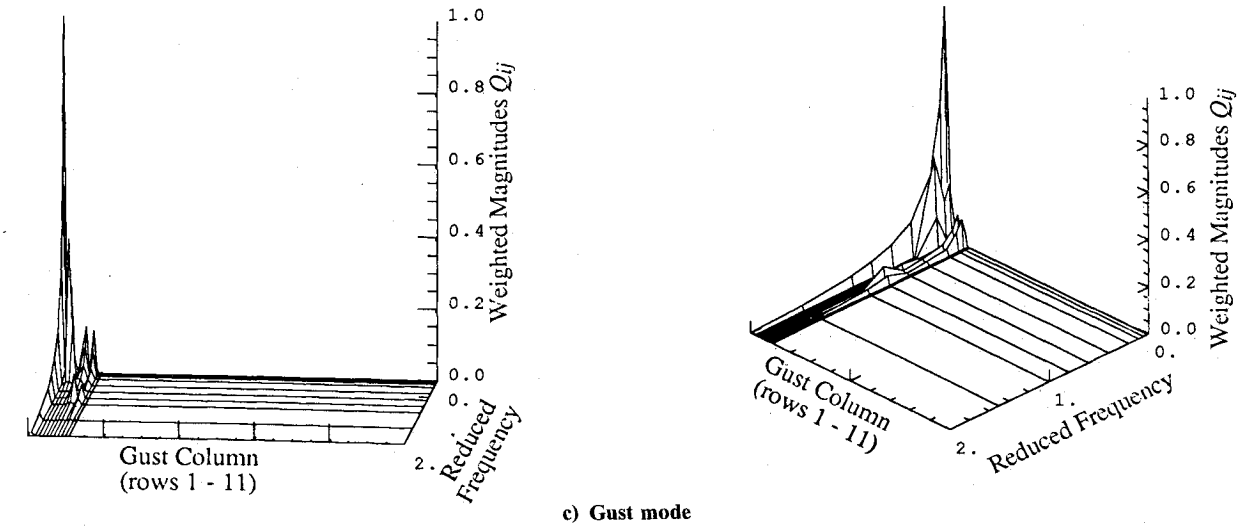

c) Gust mode

Fig. 2 Weighted magnitudes of each Q_{ij}, at each tabular reduced frequency based upon measure of importance to system characteristics near wind-tunnel limit of $q = 300$ psf.

weighted magnitude,

$$Q'_{ij} = \max_n \left\{ \mid Q_{ij}(ik_n) \mid w_{ijn} \right\}$$
$$\geq \max_n \left\{ \mid Q_{ij}(ik_n) \mid \bar{w}_{ijn} \cdot \frac{w_{cut}}{\bar{w}_{ij}} \right\} = w_{cut} \qquad (16)$$

Thus, each Q_{ij} will be at least as large as the user defined value of w_{cut}. Hence, a value of $w_{cut} = 0$ allows the full influence of physical weighting by setting the minimum equal to 0. If numerical difficulties occur, they can be resolved by assigning a small nonzero value (say 0.01) to w_{cut}, which would resolve the difficulties and still retain most physical weighting effects. A value of $w_{cut} = 1$ forces the most sensitive point for each Q_{ij} to have a weighted magnitude of 1, which normalizes each Q_{ij} with respect to its most sensitive point (the point having highest weighted amplitude) rather than its point of maximum amplitude as in standard data normalization.

The measure-of-importance, defined by Eq. (10) and used in Refs. 9–12, enforces fits almost equally over a selected frequency range of tabular values (except for equality constraints) in order to best meet the criterion for analytic continuation. Since the concept of analytic continuation, used to extend frequency domain functions into the complex plane, is approximate at best when the functions are only defined over a finite set of tabular values, physical weighting with/without optimization provides another tool for extending these functions in some reasonable fashion. Furthermore, varying the minimum of the maximum weighted magnitude, by varying the value of w_{cut} between 0 and 1, provides a mechanism that allows the approximations to incorporate a combination of physical weighting and some degree of data normalization.

Active Flexible Wing State-Space Modeling

The AFW project requires various first-order models for different purposes such as low-order models for control law design and near real-time simulation and higher-order models for control system evaluation in batch simulation. For both types of simulation it was desired to generate a reliable mathematical model in which the mass matrix was constant, i.e., had no aerodynamic terms, in order to avoid repetitive matrix inversion. This implied that the A_2 coefficients in the rational approximations had to be zero for all rigid and elastic modes. To meet the low-order requirements of design models and near real-time simulation, MS models were generated using two denominator coefficients. This resulted in an antisymmetric aeroservoelastic model with a total of 38 states. These states consisted of 22 rigid and elastic mode displacement and rate states, 12 actuator states, two gust states, and two aerodynamic states. In comparison, LS and MMP formulations using the same number of denominator coefficients in the aerodynamic transfer functions would result in antisymmetric aeroservoelastic models with a total of 58 and 60 states, respectively (22 and 24 aerodynamic states, respectively, instead of two).

Discussion of Results

The following results are for the antisymmetric AFW model at Mach 0.9. There are 11 structural modes (the roll mode is included in this group), four control modes, and one gust. In each case, the aerodynamic approximations are constrained to match the data at $k = 0$ (steady aerodynamics), the imaginary parts are matched at $k = 0.005$ (equivalent to matching quasi-steady aerodynamics), and the $A_2 = 0$. The tabulated aerodynamic data were generated using a doublet-lattice method and physically weighted with no upscaling of small weights (i.e., $w_{cut} = 0.0$).

Figure 2 is a set of three-dimensional plots (from two different views) of the physically weighted magnitudes of each $Q_{ij}(ik_n)$. These weights were determined for a value of dynamic pressure $\bar{q}_w$ that was a control law design point in the vicinity of flutter. The weights associated with the control surfaces were determined for a constant-gain control system with a single roll-rate measurement. The gust-related weights were determined based on the rms wing-tip acceleration response to Dryden's gust spectrum. On each plot, the weighted magnitudes of Q_{ij} (rows $i = 1$–11) are shown in a group for each column j. For the structural modes, j increments from 1 to 11, corresponding to the generalized coordinates. For the control modes, j increments from 12 to 15, corresponding to the leading-edge inboard (LEI), trailing-edge inboard (TEI), leading-edge outboard (LEO), and the trailing-edge outboard (TEO) control surfaces. There is one gust mode, corresponding to $j = 16$. The peaks correspond to the tabular values of reduced frequency of highest influence, as described above, on the system characteristics considered for the physical weighting. For example, in referring to the first group of plots (structural mode, column 1) in Fig. 2a the first curve (at the extreme left) in the group peaks at the third point. This indicates that for the roll mode (column 1) the system determinant is most sensitive to changes in the first generalized aerodynamic force coefficient (first curve) near the third k value, $k = 0.01$; i.e., the roll mode is most sensitive to errors in $Q_{11}(k_3)$.

Some of the rows have nearly zero weighted magnitudes for all values of k, which indicates that the system has minimal sensitivity to errors in these aerodynamic coefficients. If desired, a nonzero value for w_{cut} would increase the weight of these elements in the approximations. The view on the left indicates that for the structural modes, the diagonal terms, Q_{jj}, are the most sensitive; i.e., the curves corresponding to Q_{jj} contain the highest peaks for each column j corresponding to a structural mode. Referring also to Table 2 for the values of in-vacuum natural frequencies (ω_v), the view on the right indicates that the area of sensitivity is at k values near k_v of each mode. Figure 3 is a two-dimensional plot of the weighted magnitudes of the seven most sensitive structural mode curves in Fig. 2a, namely Q_{11}, Q_{33}, Q_{44}, Q_{66}, Q_{77}, Q_{99}, and $Q_{11,11}$. According to this plot, the system is most sensitive to errors in Q_{66} at reduced frequencies between 0.6 and 0.8. It should be noted that the actual peaks may fall between the tabulated k_n values. However, the exact peak values are not of particular importance in the effect of physical weighting as long as the neighboring k_n values are assigned with relatively high peaks, as is the case in Fig. 3. This figure was used to help provide some systematic engineering judgment to the selection of aerodynamic roots in lieu of using nonlinear optimization to determine an optimal selection.

Figures 2b and 2c, the control modes and gust mode for this model, have the same sensitivity range as the first five structural modes; i.e., they are not very sensitive to fits past $k = 0.6$. To obtain a reliable model for all 11 elastic modes, however, it appears that the range of tabular values ($0.0 \leq k_n \leq 2.0$) was appropriate for this configuration.

Table 2 Frequency parameters (ω_v,k_v) at $q = 0$ and (ω', k')[a] at flutter

Mode	ω_v, rad/s	k_v	ω', rad/s	k'	Most sensitive range of k[b]
1	2.39	0.009	9.34	0.034	[0.0,0.1]
2	44.13	0.159	45.37	0.164	[0.1,0.2]
3	49.37	0.178	53.93	0.195	near 0.2
4[c]	82.23	0.297	73.05	0.263	[0.2,0.3]
5	101.53	0.366	101.64	0.367	near 0.4
6	173.04	0.625	200.11	0.722	[0.6,0.8]
7	240.65	0.869	217.93	0.787	near 0.8
8	248.93	0.899	248.79	0.898	[0.8,1.0]
9	258.77	0.934	252.54	0.911	[0.9,1.0]
10	313.74	1.132	313.95	1.133	[1.0,1.2]
11	326.88	1.180	348.58	1.258	near 1.2

[a]ω', k'; modal frequencies and modal reduced frequencies when system goes unstable. [b]Range of k for each mode in which system determinant is most sensitive to error. [c]Flutter mode.

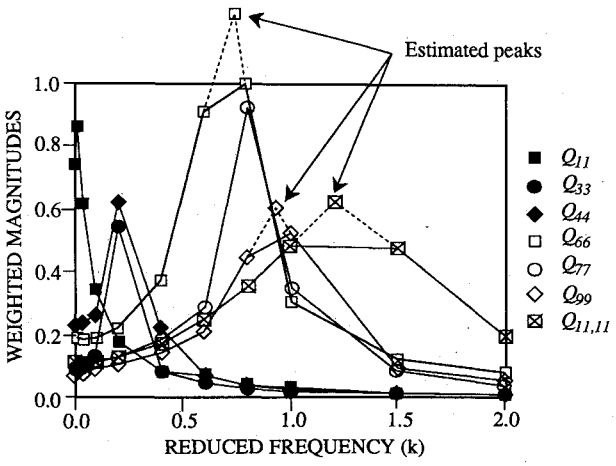

Fig. 3 Weighted magnitudes of seven most critical aerodynamic elements based upon measure of importance to system characteristics near wind-tunnel limit of q = 300 psf.

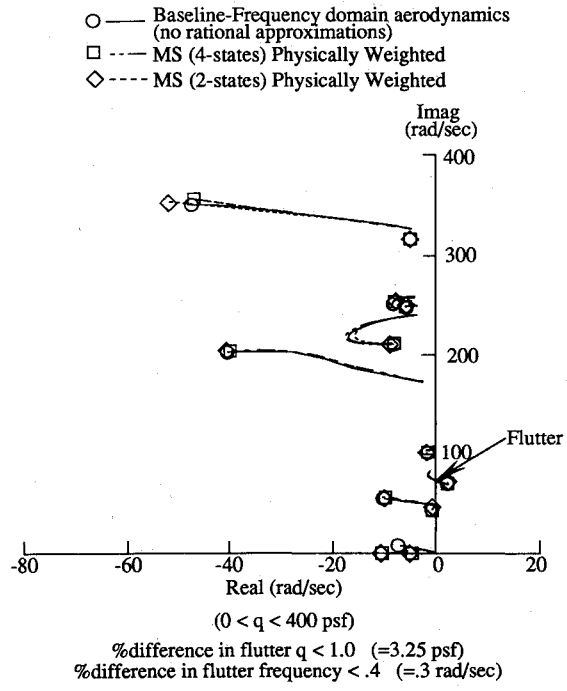

Fig. 4 Stability analysis root loci for the AFW antisymmetric modes at Mach 0.9.

The determination of an optimal set of denominator coefficients for an LS fit is a fairly quick process.[10] For the MS approximation, however, optimization of the denominator coefficients requires a three-fold iteration process in conjunction with nonlinear optimization methods, and can be time-consuming. Table 3 lists various selections of denominator coefficients based on sensitivity results from Fig. 3. The selections, although not optimal, produced good fits, and results are presented in Table 3 and Fig. 4.

Table 3 shows the choices made for the order of approximation (the number of denominator coefficients) equal to 1, 2, and 4. Also listed are the method for selection and the percent errors in flutter q and frequency. The word "unconstrained" refers to k values for which the Q_{ij} are not constrained; i.e., those other than $k = 0$ and $k = 0.005$. The words "estimated most sensitive Q_{ij}" refers to a case in which the estimated peaks (as identified in Fig. 3) are used to determine the most sensitive Q_{ij}. The k values corresponding to the "estimated peaks" are also estimated.

Figure 4 shows the open-loop root loci of a baseline configuration and the best overall of the two- and four-aerodynamic state cases as indicated in Table 3. The baseline used the tabular, frequency domain generalized aerodynamic forces and was generated using a p-k determinant iteration process employing interpolated (cubic spline) values.[9] The other two were based on linear time-invariant state-space methods. The Hassig form of implementation of the p-k method[17] becomes less accurate as the approximation $Q(p) \approx Q(0 + ik)$ degrades; hence, the baseline result for the low-frequency roll mode in Fig. 4 should not be regarded as accurate. It should be noticed that good agreements are obtained in the entire range of dynamic pressure ($0 < q < 400$ psf) even though the physical weighting has been performed with $\bar{q}_w$ = 300 psf.

To determine sets of aerodynamic approximations that consistently improve a chosen criterion as the order of the approximation increases (i.e., with increasing number of denominator coefficients), nonlinear optimization of the denominator coefficients may be employed. In this case, the optimization criterion for goodness of fit is the total physically weighted error,

$$\epsilon_{t_0} = \epsilon_t \big|_{w_{cut}=0} \tag{17}$$

defined by Eqs. (6) and (15) with $w_{cut} = 0$. Table 4 shows the comparison of ϵ_{t_0}, the total normalized error ϵ_{t_N}, defined by Eqs. (6) and (10), and the percent error in flutter q and frequency of four optimized, physically weighted MS approximations for four different orders of fit. Figure 5 shows the decreasing total physically weighted error criterion [Eq. (17)]

Table 3 Flutter parameters for various minimum-state physically weighted approximations

Order	Values of selected denominator coefficients	Method of selection (based on Table 2 and Fig. 3)	q_f, % error	ω_f, % error
1	0.8	(Unconstrained) k of most sensitive Q_{ij}	0.06	0.27
	1.0	Midrange k	−0.07	0.29
	0.722[a,b]	k' of most sensitive Q_{ij}	0.13	0.26
	0.625	k_v of most sensitive Q_{ij}	0.24	0.25
2	0.2, 0.8[a]	(Unconstrained) k of most sensitive Q_{ij}	−0.07	0.32
	0.625, 0869	k_v of most sensitive Q_{ij}	−0.87	0.38
	0.297, 0.625	(Unconstrained) k_v of most sensitive Q_{ij}, for different j	0.32	0.12
	0.625, 1.180	k_v of estimated most sensitive Q_{ij}	−0.78	0.37
	0.4, 1.5	Midrange k of least sensitive Q_{ij}	−0.55	0.36
4	0.2, 0.6, 0.8, 1.0	(Unconstrained) k of most sensitive Q_{ij}	0.64	0.00
	0.2, 0.8, 1.0, 1.5[a]	(Unconstrained) k of most sensitive Q_{ij}, for different j	1.00	0.05
	0.2, 0.73, 0.8, 1.22	k of estimated most sensitive (unconstrained) Q_{ij}	0.59	0.01
	0.009, 0.625, 0.869, 1.180	k_v of estimated most sensitive Q_{ij}	0.09	0.12
	0.159, 0.366, 0.899, 1.132	k_v of least sensitive Q_{ij}	0.98	0.05

[a]Best frequency and damping properties at flutter for all modes for corresponding order of approximation.
[b]Very little difference overall between this and other three cases.

Table 4 Comparison of optimized physically weighted minimum-state approximations

	Values of selected denominator coefficients	Physically weighted total error, ϵ_{t_0}	Normalized total error, ϵ_{t_N}	q_f, % error	ω_f, % error
1	1.225	0.32	17.75	−0.18	0.31
2	0.438, 0.582	0.14	12.98	−0.71	0.35
3	0.431, 0.917, 1.314	0.07	19.22	0.58	−0.01
4	0.511, 0.802, 0.820, 1.505	0.06	19.87	0.07	0.09

with increasing order. The normalized errors (Table 4) are poor, indicating the physical weights provide a significantly different weighting structure than the data normalization. Furthermore, since the selection of denominator coefficients is not based on optimum values of total normalized errors, the total normalized errors do not improve with increasing order. There is also no corresponding improvement in flutter q and frequency, but Fig. 6 shows that there is an improving trend in overall frequency and damping characteristics at flutter of all of the elastic modes with increasing order as compared to the frequency domain baseline flutter root characteristics. The nonlinear optimization used herein is quite fast because three equality constraints for each fit are used to explicitly reduce the number of equations to be solved in the iteration process for $[D]$ and $[E]$. The specific constraints and reduction technique are described in Refs. 8 and 14.

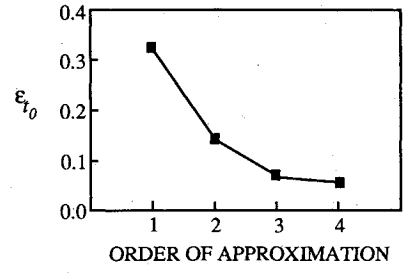

Fig. 5 Comparison of optimized total physically weighted errors with $w_{cut} = 0$ minimum-state approximations.

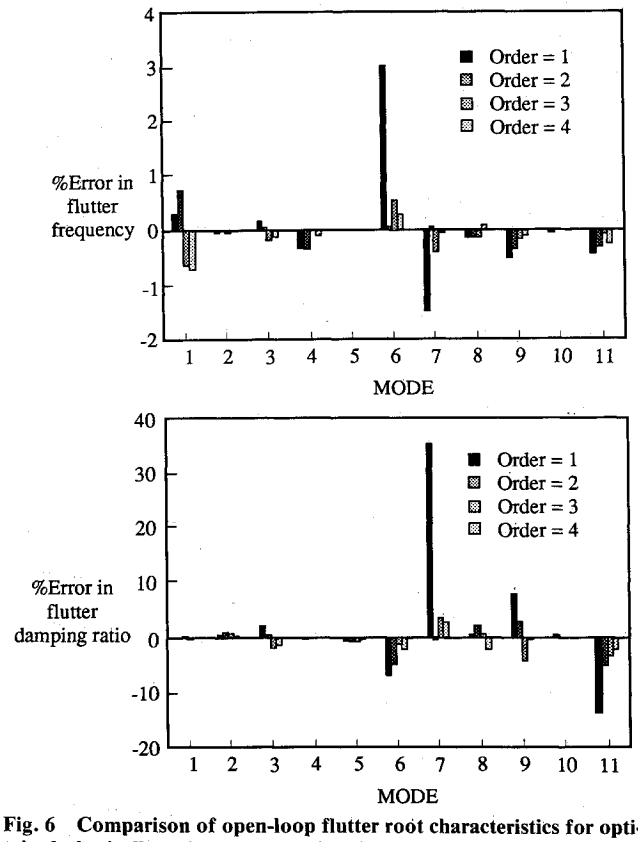

Fig. 6 Comparison of open-loop flutter root characteristics for optimized physically weighted approximations.

Figure 7 shows the stability analysis root loci of the one- and two-state optimized, physically weighted MS approximations. The figure demonstrates that the optimized one-state case matches the baseline case fairly well and that extremely close correlation is achieved with the optimized two-state approximation. In fact, the optimized two-state root loci are almost identical to the unoptimized four-state results of Fig. 4. However, the optimization only reduces the number of equations in the MS state-space formulation of the equations of motion by two. The statements made with respect to the roll-mode root locus in discussion of Fig. 4 apply here as well.

Figures 6 and 7 demonstrate that the physical weighting criterion for the structural modes is effective in achieving approximations that yield accurate stability characteristics for poles with low damping ratios. It is interesting that agreement with the p-k root loci are also good for relatively large damping ratios despite the fact that the p-k approximation $Q(p) \approx Q(0 + ik)$ is degrading; one only finds in the case of the roll mode where the p-k approximation is clearly invalid that there is no consistent improvement in damping ratio as compared to the baseline with increasing order of approximation. Results (not shown) of MS approximations with the same equality constraints shown herein, which reduce the total normalized error, ϵ_{t_N}, have slightly higher percent errors in flutter q and frequency and are much more sensitive to optimization of lag coefficients. These results indicate that physical weighting tends to improve open-loop flutter characteristics as compared to baseline frequency domain results (with cubic-spline interpolation) and to reduce the sensitivity to choices of aerodynamic roots.

Figure 8 shows the open-loop frequency response of a wingtip accelerometer to sinusoidal excitation by the outboard

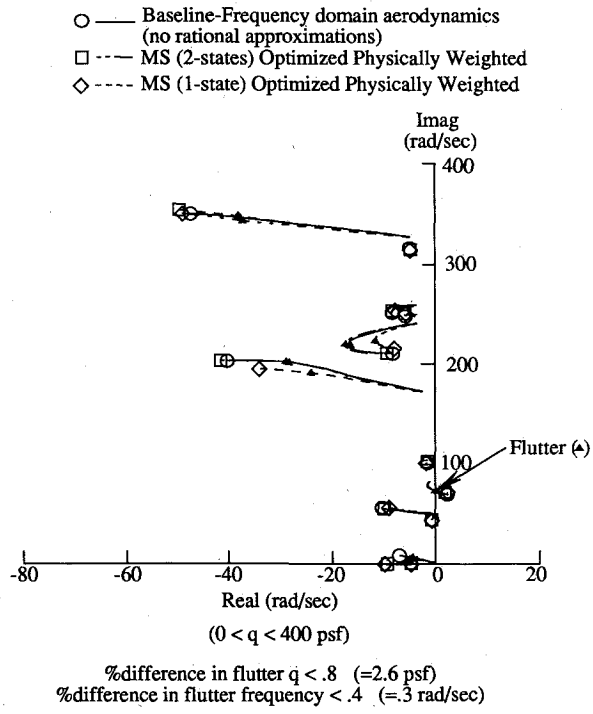

Fig. 7 Stability analysis root loci for the antisymmetric modes at Mach 0.9 using optimized physically weighted minimum-state approximations.

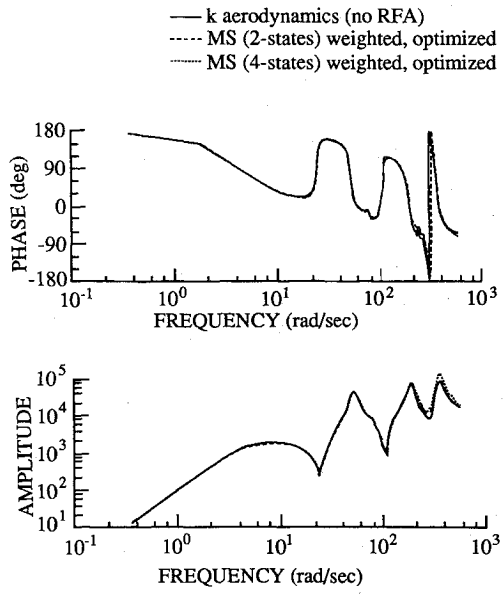

Fig. 8 Outboard-wing acceleration response to sinusoidal excitation by the outboard trailing-edge control surface.

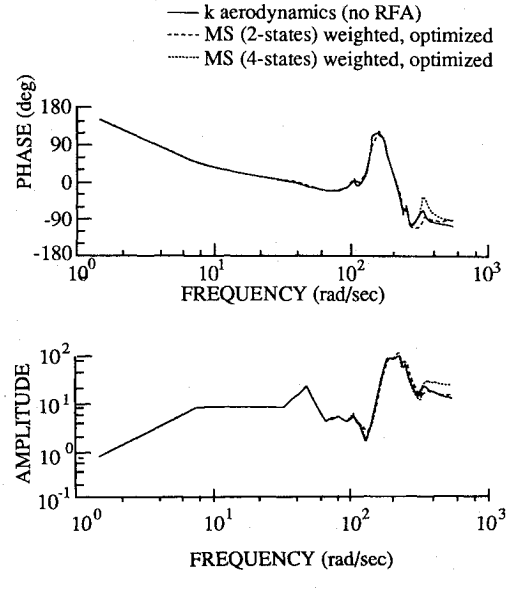

Fig. 9 Outboard-wing acceleration response to sinusoidal gust velocity at Mach 0.9 for q = 200 psf.

trailing-edge control surface at $\bar{q} = 200$ psf. The two physically weighted, optimized MS cases show excellent agreement with the response curve based on interpolation of the tabulated GAFs. Similar comparisons are shown in Fig. 9 for the response of the same accelerometer to sinusoidal gust. It may be noticed that the high-frequency responses in Figs. 8 and 9 are relatively large while the weights assigned to the high-frequency control and gust data are relatively small (Fig. 2). The small high-frequency control weights are due to the fact that the physical weighting is based in this case on the returning open-loop (actuator output) signal that includes the effects of the fuselage roll-rate measurement and the decaying actuator response, which are not considered in Fig. 8. The high-frequency gust weights are small because they are based on rms response to a gust profile that has a rapidly decaying power spectral density function, an effect which is not taken into account in Fig. 9. The good agreements shown in Figs. 8 and 9 over the entire frequency range indicate that the physically weighted aerodynamic approximations can be adequately used in subsequent aeroservoelastic analyses with control and gust parameters that are substantially different than those specified for the physical weighting.

Conclusions

By combining various capabilities, namely the minimum-state formulation of the aerodynamic approximations in the equations of motion, selectable constraints, optimal selection of denominator coefficients, as well as the determination and use of critical frequency ranges for approximating the tabular generalized aerodynamic forces based upon systematic physical weighting, it is possible to obtain good, low-order state-space mathematical models for design and simulation of aeroservoelastic systems. A physically weighted, MS state-space model with only two optimized aerodynamic states predicted a flutter dynamic pressure of a realistic case with less than 0.8% error and showed good agreement in the root loci of all elastic modes as compared to conventional stability analysis. Excellent agreements were also obtained for frequency responses to sinusoidal control surface and gust excitations over the entire frequency range of interest. The results exhibit low sensitivity to variations of the aerodynamic root selection; however, optimization does provide a mechanism for consistent improvement of overall open-loop characteristics with increasing order of the aerodynamic transfer function denominators. Furthermore, the results show a high level of accuracy over a wide range of dynamic pressure, control, and gust variables compared to baseline frequency domain results with cubic-spline interpolation. The significance of these results is that good state-space models with good open-loop characteristics can be developed having an order of magnitude fewer augmenting aerodynamic equations than more traditional approaches. This reduction facilitates the design of lower-order control systems, analysis of control system performance, and near real-time simulation of aeroservoelastic phenomena.

References

[1]Sevart, F. D., "Development of Active Flutter Suppression Wind-Tunnel Testing Technology," Air Force Flight Dynamics Laboratory, Wright-Patterson Air Force Base, OH, Rept. AFFDL TR-74-126, Jan. 1975.

[2]Roger, K. L., "Airplane Math Modeling Methods for Active Control Design," *Structural Aspects of Active Controls*, AGARD CP-228, Aug. 1977, pp. 4-1-4-11.

[3]Vepa, R., "Finite State Modeling of Aeroelastic Systems," NASA CR-2779, Feb. 1977.

[4]Edwards, J. W., "Unsteady Aerodynamic Modeling and Aeroelastic Control," SUDAAR-504 (NASA Grant NGL-05-020-007), Dept. of Aeronautics and Astronautics, Stanford University, Stanford, CA, Feb. 1977; see also NASA CR-148019.

[5]Abel, I., "An Analytical Technique for Predicting the Characteristics of a Flexible Wing Equipped with an Active Flutter-Suppression System and Comparison with Wind-Tunnel Data," NASA TP-1367, Feb. 1979.

[6]Dunn, H. J., "An Analytical Technique for Approximating Unsteady Aerodynamics in the Time Domain," NASA TP-1738, Nov. 1980.

[7]Dunn, H. J., "An Assessment of Unsteady Aerodynamic Approximations for Time Domain Analysis," *Proceedings of the Aeroservoelasticity Specialist Meeting*, Vol. 1, AFWAL-TR-84-3105, Air Force Wright Aeronautical Lab., Wright-Patterson AFB, OH, Oct. 1984, pp. 98-115.

[8]Karpel, M., "Design for Active and Passive Flutter Suppression and Gust Alleviation," NASA CR-3482, Nov. 1981.

[9]Adams, W. M., Jr., Tiffany, S. H., Newsom, J. R., and Peele, E. L., "STABCAR: A Program for Finding Characteristic Roots of Systems Having Transcendental Stability Matrices," NASA TP-2165, June 1984.

[10]Tiffany, S. H., and Adams, W. M., Jr., "Fitting Aerodynamic Forces in the Laplace Domain: An Application of a Nonlinear Nongradient Technique to Multilevel Constrained Optimization," NASA TM-86317, Oct. 1984.

[11]Tiffany, S. H., and Adams, W. M., Jr., "Nonlinear Programming Extensions to Rational Function Approximations of Unsteady Aerodynamics," AIAA Paper 87-0854-CP, April 1987.

[12]Tiffany, S. H., and Adams, W. M., Jr., "Nonlinear Program-

ming Extensions to Rational Function Approximation of Unsteady Aerodynamic Forces," NASA TP-2776, July 1988.

[13]Karpel, M., "Time-Domain Aeroservoelastic Modeling Using Weighted Unsteady Aerodynamic Forces," *Journal of Guidance, Control, and Dynamics,* Vol. 13, No. 1, 1990, pp. 30-37.

[14]Karpel, M., and Hoadley, S. T., "Physically Weighted Minimum-State Unsteady Aerodynamic Approximations," NASA TP-3025, March 1991.

[15]Noll, T. E., Perry, B., III, Hoadley, S. T., et al., "Aeroservoelastic Wind-Tunnel Investigations Using the Active Flexible Wing Model—Status and Recent Accomplishments," AIAA Paper 89-1168-CP, April 1989; see also NASA TM-101570, April 1989.

[16]Perry, B., III, Mukhopadhyay, V., Hoadley, S. T., Cole, S. R., Buttrill, C. S., and Houck, J. A., "Digital-Flutter-Suppression-System Investigations for the Active Flexible Wing Wind-Tunnel Model," AIAA Paper 90-1074-CP, March 1990; see also NASA TM-102618, March 1990.

[17]Hassig, H. J., "An Approximate True Damping Solution of the Flutter Equation by Determinant Iterarion," *Journal of Aircraft*, Vol. 8, No. 11, 1971, pp. 885–889.